**УДК 629.429.3:621.313** **doi: 10.20998/2313-8890.2025.12.02**

**Lakusta Denys**, Postgraduate student of the Department of Electromechanics and Railway Rolling Stock, +38(097)098-34-31, dennikslak@gmail.com, ORCID ID: 0009-0000-6563-757X
*National Transport University*
*1 M. Omelyanovicha-Pavlenko St., Kyiv, 01010, Ukraine*

# OPTIMIZATION OF QUASI-STEADY-STATE OPERATING MODES OF SYNCHRONOUS JET MOTORS WITH PERMANENT MAGNETS FOR ELECTRIC BUSES

***Abstract.*** *The work improves the fractional order moment method for monitoring the presence of rotor defects in induction motors. On its basis, an algorithm for diagnosing the rotor of induction motors has been developed. As a result of simulation modeling in the MATLab software environment, time dependences of the phase currents of the stator of an induction motor were obtained in the absence of a defect and in the event of damage to 1 rotor core. For the above cases, based on the proposed algorithm, generalized mean functions (GMFs) were calculated and their dependences on the order of moments were plotted. It was found that the GMF for an induction motor with damage to 1 rotor core has a greater slope than the GMF of an induction motor without a defect. According to the proposed algorithm, this is a diagnostic symptom of a defect in the rotor of an induction motor.*
***Keywords:*** *rolling stock, induction motor, diagnostics, fractional order moment method, generalized mean function*

**Лакуста Денис Іванович**, аспірант кафедри електромеханіки та рухомого складу залізниць, +380970983431, dennikslak@gmail.com@gmail.com, ORCID ID: 0009-0000-6563-757X
*Національний транспортний університет*
*вул. М. Омеляновича-Павленка, 1, м. Київ, 01010 Україна*

# РОЗВИТОК МЕТОДУ МОМЕНТІВ ДРОБОВОГО ПОРЯДКУ ТА РОЗРОБКА АЛГОРИТМІВ НА ЙОГО ОСНОВІ ДЛЯ ДІАГНОСТИКИ ЕЛЕКТРОДВИГУНІВ

***Анотація.*** *В роботі вдосконалено метод моментів дробового порядку для проведення моніторингу наявності дефектів ротора в асинхронних електродвигунах. На його основі розроблено алгоритм проведення діагностики ротору асинхронних електродвигунів. В результаті імітаційного моделювання в програмному середовищі MATLab отримано часові залежності фазних струмів статора асинхронного двигуна при відсутності дефекту та при ушкодженні 1 стрижня ротора. Для зазначених випадків на основі запропонованого алгоритму розраховано функції узагальненого середнього (ФУС) та побудовано їх залежності від порядку моментів. Встановлено, що ФУС для асинхронного двигуна при ушкодженні 1 стрижня ротора має більший нахил, ніж ФУС асинхронного двигуна без дефекту. У відповідності до запропонованого алгоритму це є діагностичним симптомом наявності дефекту в роторі асинхронного двигуна.*
***Ключові слова:*** *рухомий склад, асинхронний двигун, діагностика, метод моментів дробового порядку, функція узагальненого середнього.*

**Introduction.** The use of a diagnostic system [1] as part of the traction drive of rolling stock is one of the approaches to improving its operational efficiency. Such systems are referred to as online diagnostic systems. The rotor of an induction motor (IM) is one of its most failure-prone components [2]. The continuous variation of rolling stock operating modes significantly complicates the extraction of diagnostic symptoms of the induction motor. This is caused by continuous changes in key operational parameters, such as stator phase currents, electromagnetic torque and shaft rotational speed. In addition, the continuous variation of operating regimes of rolling stock leads to persistent transient processes in the traction drive circuits, which further complicates the acquisition of reliable diagnostic information [3]. Therefore, the selection of appropriate methods for processing diagnostic information in the design of online diagnostic systems constitutes a relevant and important research task.

**Analysis of Previous Research.** In [4], existing methods for processing current signals intended for solving the tasks of monitoring and diagnostics of the technical condition of the IM rotor are considered. There also exist other modern and promising signal processing methods that have not previously been applied to these tasks, including: non-orthogonal combined Fourier analysis of smoothed signals [5, 6], non-orthogonal amplitude and frequency analysis of smoothed signals [7, 8], comparative analysis of positive and negative fluctuations [9, 10], fractional moment statistics [11, 12].

Non-orthogonal combined Fourier analysis of smoothed signals represents one of the approaches within non-orthogonal amplitude and frequency analysis. In this approach, the signal frequencies are determined using the Fourier transform; subsequently, the harmonics with the largest amplitudes are selected, after which the amplitudes of the selected harmonics are approximated using the least squares method [5, 6].

This approach allows the investigated signal to be described by a small number of parameters corresponding to the number of selected harmonics of the Fourier spectrum. The method can therefore be applied to information compression tasks. It

is characterized by low computational complexity, $O = (n \cdot log(n))$, which enables its implementation in continuous-mode technical condition monitoring systems based on microcontrollers. However, this method is not suitable for solving the problem of electric motor diagnostics, since the frequencies it "detects" are determined by the Fourier transform, which requires a large time window, on the order of approximately 100 seconds [6]. A 100-second time window requires several megabytes of memory, which is critically excessive for low-power systems based on microcontrollers.

Non-orthogonal amplitude and frequency analysis of smoothed signals represents a new approach to signal representation with trends and is free from assumptions regarding the signal model [7, 8]. This method constitutes a novel approach to discrete spectral analysis of random signals and fluctuations. The approach is based on the successful solution of a modified Prony problem for strongly correlated random sequences [13, 14]. In contrast to the classical Prony method, where the set of frequencies is assumed to be unknown [4], the proposed approach enables the distribution of unknown frequencies to be determined for correlated random sequences. Prior information about the frequency distribution simplifies calculations and provides additional stability in the presence of noise. The method uses only the informatively significant frequency band, which allows highly accurate fitting of the target signal. This implies that any random signal measured in the time domain can be identified in the frequency domain without model assumptions related to the frequency-domain behaviour of the signal. The method overcomes the fundamental limitations of the conventional Prony method. Its disadvantages include high computational complexity, $O = (n^4)$; therefore, this method is not suitable for implementation in continuous-mode technical condition monitoring systems for induction motors based on microcontrollers.

Comparative analysis of positive and negative fluctuations makes it possible to represent signals in the form of ten statistical parameters for the comparison and clustering of random signals [9, 10]. This approach is free from processing errors and data model assumptions. Due to its low computational complexity, its implementation is appropriate in continuous-mode data processing systems based on

microcontrollers. This approach has also been considered as a potential data processing method for continuous-mode monitoring systems of induction motors. The drawback of this method is the need to conduct a large series of experiments to study the dependencies of the method parameters on various parameters of electric motors. The large number of parameters required for method implementation also complicates the decision-making system; therefore, this approach is more suitable for systems based on artificial intelligence, such as expert systems or fuzzy logic systems.

Fractional moment statistics constitutes an approach for:

- description;

- analysis and comparison of signals not only within the framework of classical statistical parameters such as arithmetic mean, root mean square, and variance (i.e., integer-order moments), but also fractional-order moments.

Within the framework of fractional moment statistics, extended equations of conventional statistical parameters have been developed, including: the generalized mean function as an analogue of the arithmetic mean, the generalized Pearson correlation coefficient, etc. These functions enable the quantitative description of signals of different lengths using a limited number of parameters and allow their mutual comparison. In [11, 12], the effectiveness of the method has been demonstrated in tasks related to diagnostics, namely in problems of identification, recognition, comparison of sequences with noise signals and sequences with noisy useful signals, as well as in information compression tasks.

Based on the conducted analysis, it can be concluded that fractional moment statistics represents the most promising approach for the analysis of induction motor signals for the purpose of solving tasks of monitoring and diagnostics of technical condition.

**Problem Statement.** The objective of this paper is to adapt the fractional-order moment method and to develop an algorithm based on it for the diagnostics of rotor faults in induction motors.

**Research Results.**

**Generalized Mean Function.** Within the framework of fractional moment statistics, the generalized mean function has been developed. The generalized mean function for a moment of order $p$ is calculated according to the following expression

$$\Delta_{\left(mom_p\right)} = \left( \frac{1}{L} \cdot \sum_{i=1}^{L} y_i^{mom_p} \right)^{\frac{1}{mom_p}}, \tag{1}$$

where: $y_i$ is the input sequence; $L$ is the number of points; $p$ =1,2,...,$P$ is the positive integer; $mom_p$ is the moment of order $p$.

The moment of order $p$ is calculated according to the following expression

$$mom_p = exp\left\{ min + \frac{p}{P} \cdot \left( max - min \right) \right\}, \tag{2}$$

*min, max* are the parameters of the generalized mean function that define the range of moments on a logarithmic scale; $P$ – is the coefficient that determines the resolution of the moment orders.

In [11, 12], the high sensitivity of the generalized mean function to small statistical differences in the compared signals is demonstrated.

**Selection and Justification of the Signal Preprocessing Method.**To calculate the parameters of fractional moment statistics, the data must be preprocessed in order to extract the diagnostically informative component from the original time-domain signals. At the same time, the preprocessing method must have acceptable computational complexity to ensure its feasibility for implementation in continuous-mode technical condition monitoring devices for electric motors based on microcontrollers.

In [4], existing methods for processing current and vibration signals of electric motors are analysed from the perspective of implementation in monitoring devices. Most existing methods are based on the use of the fast Fourier transform (FFT) in various combinations and modifications. The FFT has relatively low computational complexity, $O = (n \cdot log(n))$, which makes it convenient for implementation in the systems based on microcontrollers. Another significant advantage of the FFT is its

high degree of maturity and extensive research background – there exists a large body of publications investigating electric motor faults based on spectral analysis using the FFT.

To mitigate these limitations, resampling methods [16, 17] are commonly employed, as well as variation of the length of the analysed signal window. Resampling is an intensive operation in terms of both processing time and memory resources, since multiple FFT calculations are required to obtain harmonic amplitudes without spectral leakage effects. Therefore, the application of resampling is not considered in this paper.

Variation of the length of the analysed signal window also affects the required memory capacity and calculation time. On the one hand, a long time-domain signal window enables the acquisition of a spectrum with high frequency resolution and, at the same time:

- requires a large memory capacity;
- requires a long data acquisition time;
- increases calculation time.

On the other hand, a short signal window requires less calculation time and memory. However, the resulting spectrum exhibits low frequency resolution, and the harmonics of interest may become indistinguishable. In order to substantiate the latter statement, a signal consisting of three cosine components was investigated

$$i(t_i) = cos(2 \cdot \pi \cdot f_1 \cdot t_i) + 0.5 \cdot cos(2 \cdot \pi \cdot f_2 \cdot t_i) + 0.5 \cdot cos(2 \cdot \pi \cdot f_3 \cdot t_i), \quad (3)$$

where $f_1$ = 50 Hz; $f_2$ = 49 Hz; $f_3$ = 51 Hz.

The time variable is defined as

$$t_i = \frac{i}{f_d}, \quad (4)$$

Where: $f_d$ is the sampling frequency; $i$ = 0, 1,..., $N$; $N = f_d \cdot T$ is the number of points as a function of the selected data acquisition time interval $T$.

Fig. 1 shows signal (3) at a sampling frequency of $f_d$ = 250 Hz; the blue line

represents the original signal, while the red markers indicate the sampled values at frequency $f_d$.

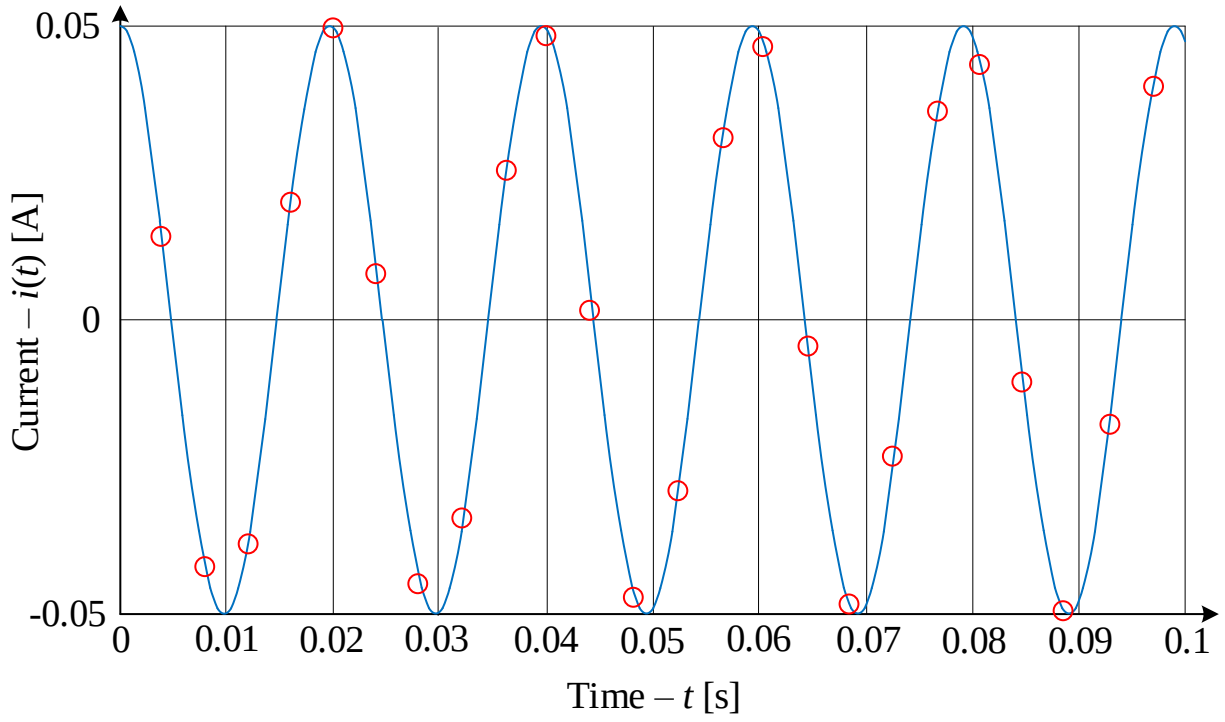


Figure 1 – Investigated test signal in the time domain

As follows from Fig. 2, for $T$ = 10 s, the FFT spectrum allows the harmonic components to be clearly distinguished from each other. However, for $T$ = 3 s and $T$ = 0.2 s, the harmonics become indistinguishable, although the latter case is more favourable in terms of information processing speed, since it requires less memory and shorter calculation time.

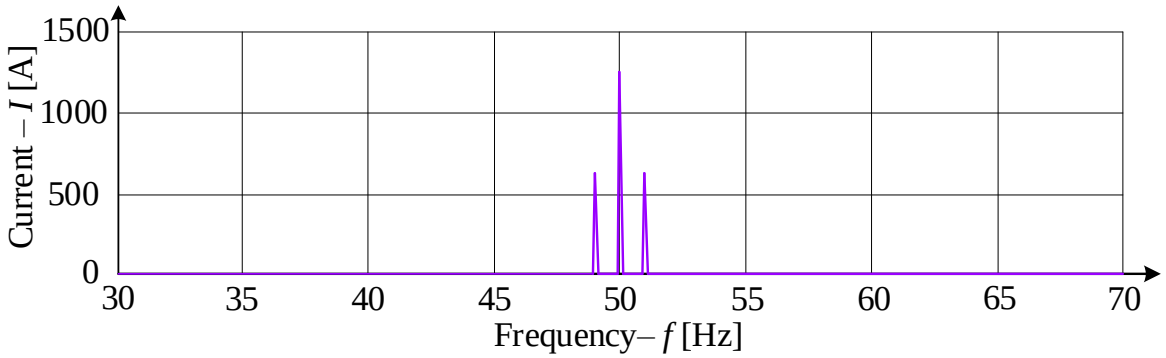


a)

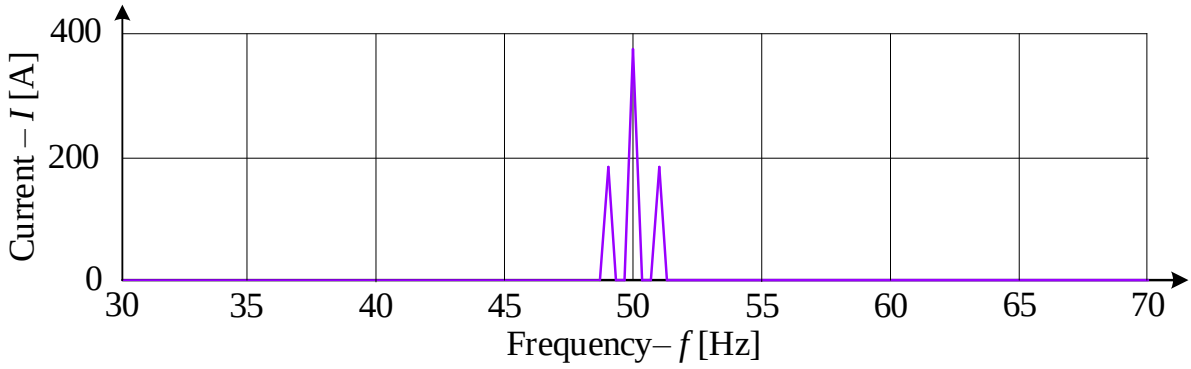


b)

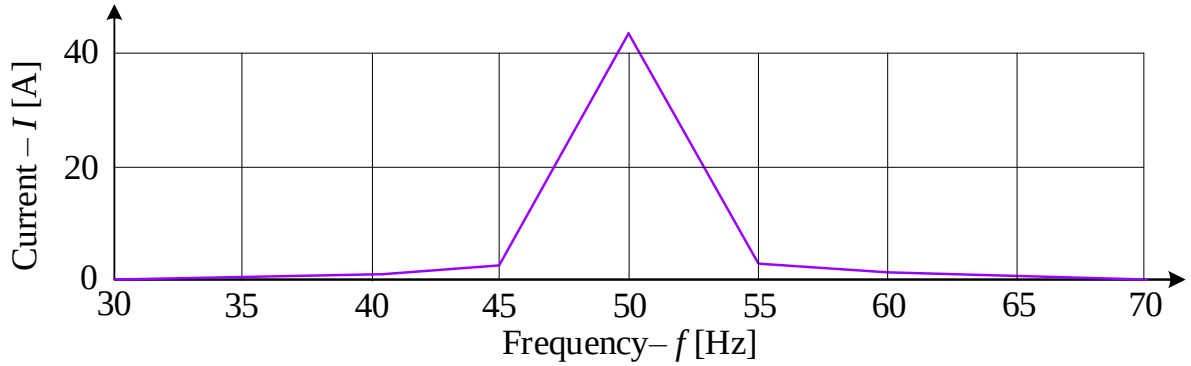


c)

Figure 2 – Amplitude and frequency spectra of signal (3) for different values of the data acquisition interval *T*: 10 s (a), 3 s (b) and 0.2 s (c).

The number of points in the FFT spectrum is equal to the number of points *N* of the analysed signal in the time domain. Therefore, the frequency resolution is equal to

$$\Delta f = \frac{f_d}{N} = \frac{f_d}{f_d \cdot T} = \frac{1}{T}. \tag{5}$$

Fig. 2 shows the amplitude spectra obtained using the FFT for different values of *T*: 0.2 s, 3 s and 10 s.

For this reason, a large time-domain signal window is required to achieve good frequency resolution of the FFT spectrum. With poor frequency resolution, the FFT spectrum does not allow closely spaced frequency components to be distinguished. In this case, the amplitudes of the true harmonic components are distributed among neighbouring harmonics of the FFT spectrum. Moreover, poor frequency resolution

leads to the spectral leakage effect, since the frequencies of the true harmonics do not coincide with the frequencies of the obtained spectrum [17]. Fault signatures become "merged" with the nearest spectral harmonics, and the amplitudes of the fault signatures are distributed around their true frequency locations. As a result, the amplitudes of the fault signatures become indistinguishable. Therefore, an additional spectral processing method is required for spectra with poor frequency resolution, which enables the detection of weak amplitude variations of harmonics located in the vicinity of fault signatures.

**Enhancement of the Fractional-Order Moment Method for Solving Rotor Diagnostics Problems in Induction Motors.** The proposed fractional-order moment method for solving tasks of monitoring and diagnostics of the technical condition of electric motors consists of the following main steps:

1. Measurement of one or more motor signals.

2. Application of the Fourier transform to the measured signal in order to represent it in the frequency domain.

3. Calculation of the generalized mean function (GMF) for the spectrum obtained at the previous stage, according to expressions (1) and (2).

4. Comparison of the obtained GMF with GMF calculated for machines in different technical conditions. If the GMF obtained for a motor in good working order is "close" to the GMF obtained for the tested motor, the motor is considered to be in good working order. Otherwise, anomalies and possible faults are assumed to be present. The method of GMF comparison and the criterion of "closeness" are defined in each specific implementation of the proposed method. Thus, in [18, 19], the tangent of the slope angle between the GMF obtained for the tested motor and the GMF obtained for a motor in good working order is calculated for comparison. To solve fault diagnostics tasks, it is necessary to obtain GMF for motors with defects and to compare the GMF of the tested motor not only with the GMF of a motor in good working order, but also with GMF obtained for motors with known defects.

The proposed method does not depend on the specific nature of the measured signal and is free from model assumptions regarding the signal.

**Development of Signal Processing Algorithms for Current and Vibration Signals for Solving Monitoring and Diagnostics Tasks of Induction Motors.**The signal processing algorithm consists of a preprocessing stage, which includes: α−β transformation, decimation, FFT and extraction of informative frequency bands (IFBs), as well as a main processing stage, which includes: Calculation of the generalized mean function (GMF), calculation of the slope of the current GMF relative to the obtained GMF and decision-making regarding the technical condition of the induction motor.

The algorithm consists of the following steps.

**Step 1.** α−β transformation. The three-phase stator currents of the induction motor are represented as a rotating space vector in a reference frame attached to the stator phase plane. The real axis α is aligned with the axis of one of the stator windings, while the imaginary axis β is phase-shifted by 90 degrees. The coordinate transformation from the measured phase currents $i_a$, $i_b$, $i_c$, to the coordinates $i_\alpha$, $i_\beta$ is defined by the following matrix operation:

$$\begin{bmatrix} i_\alpha \\ i_\beta \end{bmatrix} = \frac{2}{3} \cdot \begin{bmatrix} 1 & -\frac{1}{2} & -\frac{1}{2} \\ 0 & \frac{\sqrt{3}}{2} & -\frac{\sqrt{3}}{2} \end{bmatrix} \cdot \begin{bmatrix} i_a \\ i_b \\ i_c \end{bmatrix}. \tag{6}$$

**Step 2.** Transformation from α−β projections to the stator current space vector

The transformation from α−β projections to the stator current space vector is performed in accordance with the following expression:

$$i_s = i_\alpha + i_\beta. \tag{7}$$

**Step 3.** Decimation. Modern measurement equipment enables a significant increase in the sampling frequency. Moreover, contemporary sensor technologies allow signal acquisition at high frequencies without increasing noise levels. High-frequency information may contain diagnostically relevant content [20]. However, a high sampling frequency leads to increased memory requirements. Therefore, in the proposed method, a decimation procedure based on averaging is introduced. Thus, for

further analysis, only the averaged value of several measurements is used. For this purpose, the input sample of the output signal $i_s^T$ is represented as an observation vector

$$i_s^T = [i_{s1}, i_{s2}, ..., i_{sM}]; \tag{8}$$

$$M = T \cdot f_d, \tag{9}$$

where: $M$ is the total number of measurements; $T$ is the data acquisition time interval; $f_d$ is the original sampling frequency.

Decimation based on the averaging process produces a signal that can be represented as the observation vector $y^T$:

$$y^T = \left[ \frac{1}{k_d} \cdot \sum_{j=1}^{k_d} i_{sj}, \frac{1}{k_d} \cdot \sum_{j=1}^{2 \cdot k_d} i_{sj}, ..., \frac{1}{k_d} \cdot \sum_{j=1}^{M} i_{sj} \right]; \tag{10}$$

$$k_d = \frac{f_d}{f_{dec}}, \tag{11}$$

where $k_d$ – is the decimation factor; $F_{dec}$ is the frequency obtained after decimation.

The dimension $N$ of the vector $y^T$ after decimation is equal to

$$N = \frac{M}{k_d}. \tag{12}$$

For further processing, it is sufficient to store only the signal $y$, represented by a data buffer of dimension $N$, which is $k_d$ times smaller than the original vector $i_s^T$.

**Step 4.** Fast Fourier transform. The calculation of the full signal spectrum is performed using the FFT, in accordance with the following expression [21]:

$$FFTfull_k = \left| \frac{1}{\sqrt{N}} \cdot \sum_{n=1}^{N} y_j \cdot e^{\frac{(-2 \cdot \pi \cdot j) \cdot (n-1) \cdot (k-1)}{N}} \right|; \tag{13}$$

$$full_k = k \cdot \frac{F_{dec}}{N}, \tag{14}$$

where: $y$ – is the signal after decimation; $N$ – is the number of pints after decimation; $FFTfull_k$ is the modulus of the amplitudes of the full Fourier spectrum; $full_k$ – is the frequency of the full Fourier spectrum; $k = 1,2, ..., N$.

In order to avoid treating the true and imaginary parts separately, the modulus is used.

**Step 5.** Extraction of the informative frequency band. The informative frequency band (IFB) is a segment of the Fourier spectrum limited to a specific frequency range. The frequency range itself is selected based on the type of the analysed defect. This makes it possible to reduce the required calculation load while increasing the sensitivity of the method, since non-informative harmonics are excluded from the calculation of the generalized mean function (GMF). Each defect affects the spectrum of induction motor signals in a different manner. In order to analyse only the informative part of the spectrum, a procedure for IFB extraction is introduced. The IFB depends on:

- the supply voltage frequency;
- the type of the analysed fault;
- the resulting frequency after decimation.

The extraction of the IFB is performed in accordance with the following expression

$$IFR_l = FFTfull_p; \tag{15}$$

$$l = 1,2,3,..., p_{max} - p_{min}; \tag{16}$$

$$p = p_{max} - p_{min}; \quad p_{min} = floor\left( f_{min} \cdot \frac{N}{F_{dec}} \right); \quad p_{max} = floor\left( f_{max} \cdot \frac{N}{F_{dec}} \right), \tag{17}$$

where: $IFR$ – is the segment of the Fourier spectrum included in the IFB; $f_{min}$ – is the lower limit of the IFB; $f_{max}$ – if the upper limit of the IFB; $floor()$ – is the operation of rounding to integer.

**Step 6.** Calculation of the generalized mean function. The GMF is calculated for the segments of the Fourier spectrum that belong to the IFB, in accordance with

the following expression

$$\Delta_{\left(mom_p\right)} = \left( \frac{1}{L} \cdot \sum_{i=1}^{L} IFR_i^{mom_p} \right)^{\frac{1}{mom_p}}, \tag{18}$$

where: $L$ – is the number of harmonics included in the considered spectrum segment within the IFB; $mom_p$ is the order of moment, which can be calculated as:

$$mom_p = exp\left\{ min + \frac{p}{P} \cdot \left( max - min \right) \right\}, \tag{19}$$

where: *min*, *max* and $P$ are the parameters of the GMF; $p$ =1,2,...,$P$.

The values of *min* and *max* define the range of considered moments, while $P$ – is the coefficient that determines the resolution of the orders of moment.

**Step 7.** Comparison of GMF slopes and technical condition assessment. At this stage, the calculated GMF slopes are compared with predefined reference values obtained for induction motors in different operating states. First, the obtained slopes are checked for compliance with a predefined confidence interval, which is determined empirically. If the slopes fall outside this interval, it is concluded that the technical condition of the induction motor is not normal. In this way, continuous-mode technical condition monitoring of the induction motor is implemented. Based on this comparison, a final conclusion is made regarding the technical condition of the tested motor.

## Results of Modelling and Discussion.

The object of the study is the CTA-1200 induction motor, which is used as a traction motor in DS-3 series electric locomotives operated by PJSC “Ukrzaliznytsia”. The parameters of the CTA-1200 induction motor are presented in Table 1 [22]. In [22], a simulation model of the induction motor of this series is presented, implemented in the MATLab software environment. This simulation model allows modification of the geometric parameters of the motor, including, in particular, the specification of the number of damaged rotor bars. For this reason, the indicated simulation model of the induction motor was selected for conducting the

present study. Since the structure of the CTA-1200 induction motor simulation model is presented in [22], it is not reproduced in this paper.

Table 1 – Parameters of the CTA-1200 induction motor [22]

| Parameter | Unit of measurement | Value |
|---|---|---|
| Shaft power rating, $P_n$ | kW | 1200 |
| Rated phase voltage, $U_n$ | V | 1527 |
| Rated frequency of supply voltage, $f_s$ | Hz | 55.8 |
| Nominal motor shaft speed $n_n$ | rpm | 1110 |
| Rated torque on the motor shaft $T_n$ | N·m | 10417 |
| Number of poles $p$ | r.u. | 6 |
| The number of turns of the stator winding $w_s$ | r.u. | 48 |
| Number of rotor bars $N_r$ | r.u. | 64 |
| Stator winding active resistance $r_s$ | Ω | 0.0226 |
| Rotor winding active resistance $r_s$ | Ω | 0.0261 |
| Dissipation inductance of the stator phase $L_{\sigma s}$ | mH | 0.65 |
| Dissipation inductance of the rotor phase $L_{\sigma r}$ | mH | 0.45 |
| Inductance of the magnetic circuit $L_{\mu}$ | mH | 19.4336 |
| Moment of inertia $J$ | kg·m$^2$ | 39 |

The study was conducted as follows. Time-domain waveforms of the stator phase currents of the induction motor were obtained for a motor in good operating order and for a motor with one damaged rotor bar. Subsequently, in accordance with expressions (6) and (7), the time-domain waveforms of the stator phase current space vector were obtained for the specified cases. Further analysis showed that the most informative among the short time windows is a window with a duration of 0.448 s. For a window of this duration, decimation was performed. The decimation frequency was selected as $f_{dec}$ = 1116 Hz. The time-domain waveforms of the stator current space vectors after decimation for both cases are shown in Fig. 3.

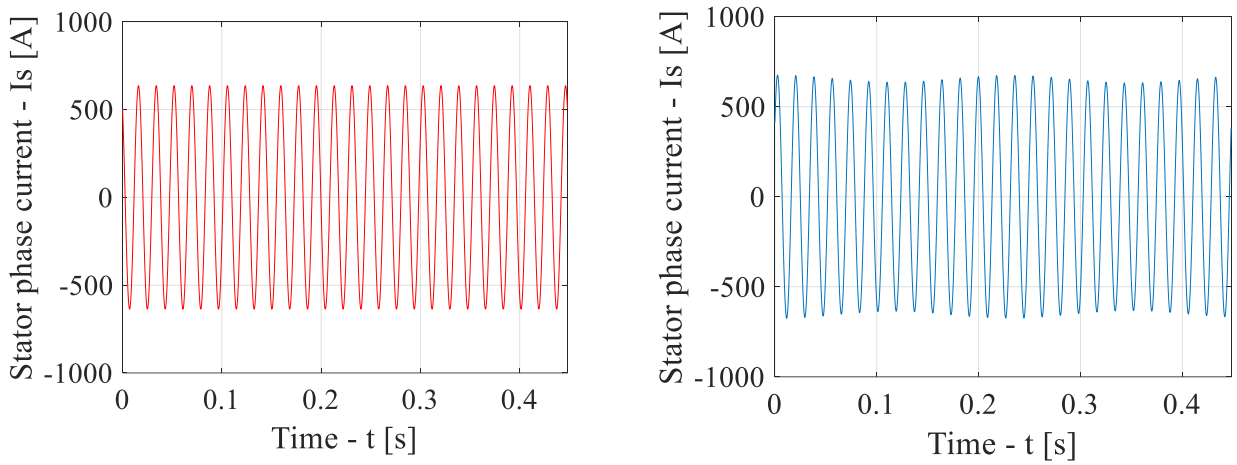


Figure 3 – Time-domain waveforms of the stator current space vectors after decimation: motor without defects (a) and motor with one damaged rotor bar (b).

The amplitude and frequency spectra of the stator current space vectors were calculated and plotted for both cases. In accordance with expressions (15)–(17), the informative frequency band (IFB) was selected. For the IFB, the boundary frequencies were determined as $f_{min}$ = 50,0 Hz and $f_{max}$ = 61,6 Hz. The amplitude and frequency spectra of the stator phase current space vectors for the selected informative frequency band are shown in Fig. 4.

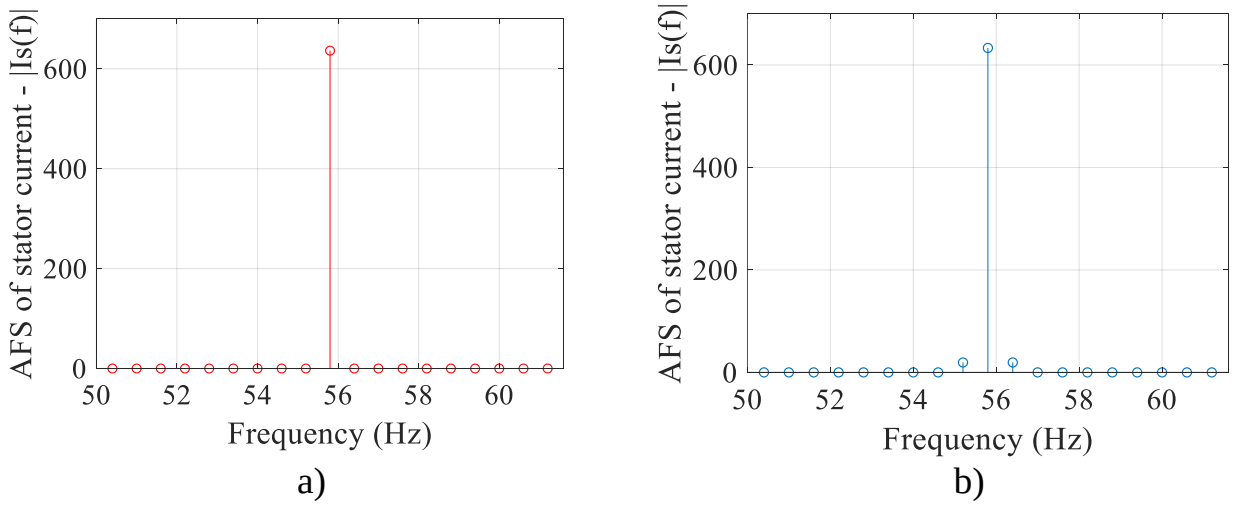


Figure 4 – Amplitude and frequency spectra of the stator current space vectors for the informative frequency band: motor without defects (a) and motor with one damaged rotor bar (b).

From Fig. 4, the frequencies of the sideband harmonics, which are indicative of the presence of rotor defects in an induction motor, were identified. In accordance

with [23], the values of these frequencies can be determined as:

$$f_{brb} = f_s \pm f_r, \tag{20}$$

where $f_r$ is the rotor rotational subharmonic frequency, defined as [23]

$$f_r = 2 \cdot s \cdot f_{snom}, \tag{21}$$

where: $f_{snom}$ is the nominal stator supply frequency; $s$ is the slip, determined according to the expression

$$s = \frac{n_s - n_{snom}}{n_s}, \tag{22}$$

where $n_s$ is the synchronous rotor speed (Table 1); $n_{som}$ is the rotor speed at nominal stator supply frequency (Table 1).

The values of the sideband harmonic frequencies obtained by calculation and determined experimentally are listed in Table 2.

Table 2 – Sideband harmonic frequencies obtained by calculation and determined experimentally

| Method | Left sideband frequency, $f_{brbl}$ Hz | Right sideband frequency, $f_{brbr}$ Hz | Error, σ % |
|---|---|---|---|
| Calculation | 55,22 | 56,38 | 0,04 |
| Simulation modelling | 55,2 | 56,4 | 0,035 |

Analysis of the results presented in Table 2 demonstrates the high accuracy of the obtained spectral components of the stator current space vector spectrum for the motor with one damaged rotor bar.

In accordance with expressions (18) and (20), the generalized mean functions (GMFs) were calculated for the motor without defects and for the motor with one damaged rotor bar. The following parameters were selected for the GMF calculation: the range of moments $p_{min}$ = -15, $p_{max}$ = 15 $P$ = 30. The GMFs for the investigated cases are shown in Fig. 5, a. Fig. 5, b shows the upper parts of the GMFs.

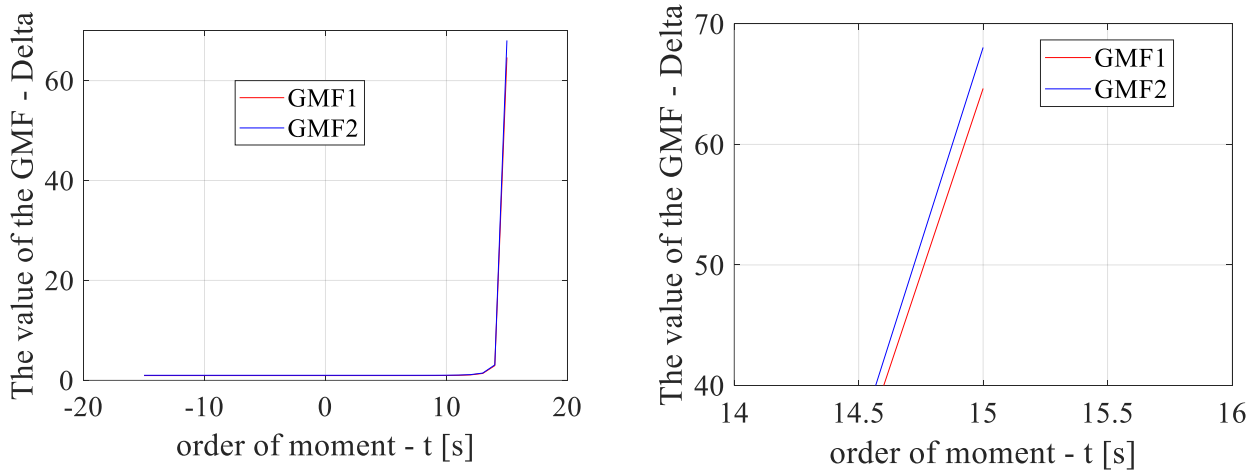


Figure 5 - GMFs for the investigated cases: full GMFs (a) and upper part of the GMFs (b).

Fig. 5 has the the following notation: GMF1 – GMF of the motor without defects; GMF2 – GMF of the motor with one damaged rotor bar.

As can be seen from Fig. 5, b, the GMF of the motor with one damaged rotor bar has a greater slope than the GMF of the motor without defects. This feature serves as a diagnostic indicator of the presence of a rotor defect in the investigated induction motor.

## Conclusions

The fractional-order moment method has been enhanced for the purpose of monitoring induction motors with respect to the detection of rotor defects.

Based on the enhanced fractional-order moment method, a diagnostic algorithm for induction motors has been proposed for detecting the presence of rotor defects.

Simulation modelling of the CTA-1200 induction motor, used as a traction motor in DS-3 series electric locomotives operated by PJSC “Ukrzaliznytsia”, was performed in the MATLab software environment.

As a result of the simulation modelling, time-domain waveforms of the stator phase currents of the induction motor were obtained for both the case of a motor in good operating order and the case of a motor with one damaged rotor bar.

For both cases, the generalized mean functions (GMFs) were calculated and their dependencies on the moment order were constructed. It was established that the

GMF of the induction motor with one damaged rotor bar exhibits a greater slope than the GMF of the motor in good operating order. In accordance with the developed algorithm, this feature constitutes a diagnostic symptom indicating the presence of a rotor defect in the induction motor. Thus, the proposed method and the developed algorithm can be effectively used for monitoring and diagnostics of rotor defects in induction motors.

**БІБЛІОГРАФІЧНИЙ СПИСОК:**

1. Komorski P., Kominowski J., Motyl M. (2022). A proposal for a mobile system of vehicle and rail track diagnostics. *Transport Problems, 17*(2), 46–56. https://doi.org/10.20858/tp.2022.17.2.04
2. Gubarevych O., Goolak S., Golubieva S. (2022). Systematization and selection of diagnosing methods for the stator windings insulation of induction motors. *Revue Roumaine des sciences techniques—série électrotechnique et énergétique*, 67(4), 445–450.
3. Goolak S., Gorobchenko O., Holub H., Dudnyk Y. (2024). Increasing the efficiency of railway rolling stock operation with induction traction motors due to implementation of the operational system for diagnostic condition of rotor. *Diagnostyka*, 25(4), 1–11. https://doi.org/10.29354/diag/193809
4. Goolak S., Gubarevych O., Yurchenko V., Kyrychenko M. (2025). A review of diagnostic information processing methods in the construction of systems for operating diagnostics of rotor eccentricity of induction motors. *Diagnostyka*, 26(1), 1–15. https://doi.org/10.29354/diag/202757
5. Kumar A., Nanthaamornphong A., Gaur N., Masud M. (2025). Low complexity hybrid algorithm for improving PAPR BER and PSD in OTFS under diverse channel conditions. *Scientific Reports*, 15(1). 42023. https://doi.org/10.1038/s41598-025-26748-w
6. Mushtaq U., Khan A. A., Baig S., Ahmad M., Ribeiro M. V. (2025). SWIPT Enabled Wavelet Cooperative NOMA: Energy-Efficient Design Under Imperfect SIC. *Electronics*, 14(22). 4390. https://doi.org/10.3390/electronics14224390
7. Song Y., Yan J., Duan Z., Zhang L. (2025, July). Position Identification of Pmsm Based on Second-Order Generalized Integrator Under Hall Sensors Fault. In *2025 4th Conference on Fully Actuated System Theory and Applications (FASTA)* (pp. 1026–1031). IEEE. 10.1109/FASTA65681.2025.11138642
8. Liu H., Yang K., Liu L., Zheng Y., Cao X., Sun W., Zheng Y. (2025). Optimization of Energy Management Strategy for Hybrid Power System of Rubber-Tyred Gantry Cranes Based on Wavelet Packet Decomposition. *Energies*, 19(1), 139. https://doi.org/10.3390/en19010139
9. Tong F., Dong S., Lai J., Yuan X., Li X. (2022). Wall shear stress and wall heat flux in a supersonic turbulent boundary layer. *Physics of fluids*, 34(1). 015127. https://doi.org/10.1063/5.0079230
10. Andronis V., Karathanassi V., Tsalapati V., Kolokoussis P., Miltiadou M., Danezis C. (2022). Time series analysis of landsat data for investigating the relationship between land surface temperature and forest changes in Paphos Forest, Cyprus. *Remote Sensing*, 14(4), 1010. https://doi.org/10.3390/rs14041010
11. Wang Z. Z., Goh S. H. (2022). A maximum entropy method using fractional moments and deep learning for geotechnical reliability analysis. *Acta Geotechnica*, 17(4), 1147–1166. https://doi.org/10.1007/s11440-021-01326-2
12. Destrempes F., Cloutier G. (2023). Review of envelope statistics models for quantitative ultrasound imaging and tissue characterization. In *Quantitative ultrasound in soft tissues* (pp. 107–152). Cham: Springer International Publishing. https://doi.org/10.1007/978-3-031-21987-0_7

13. Plonka G., Potts D., Steidl G., Tasche M. (2023). Prony method for reconstruction of structured functions. In *Numerical Fourier Analysis* (pp. 567–620). Cham: Springer International Publishing. https://doi.org/10.1007/978-3-031-35005-4_10
14. Rozgić D., Petrović P. B. (2022). New modified DFT-Prony-based algorithms for removal of decaying DC components from fundamental phasor estimates. *Electrical Engineering*, 104(5), 3265–3279. https://doi.org/10.1007/s00202-022-01548-x
15. Aguilar J., Paulus L., Werbunat D., Grathwohl A., Waldschmidt C. (2025, March). Radon-Fourier Transform for Timing Correction in Uncoupled Digital Radar Networks. In *2025 16th German Microwave Conference (GeMiC)* (pp. 415–418). IEEE. https://doi.org/10.23919/GeMiC64734.2025.10979010
16. Xu T., Liu Y., Cui J., Jiang Y., He M., Miao D., Liu W., Li J. (2025). Calibration methods of optical path difference in optical frequency scanning interferometry with resampling resolving. *Measurement*, 248, 116854. https://doi.org/10.1016/j.measurement, 2025.116854
17. Niu G., Dong X., Chen Y. (2023). Motor fault diagnostics based on current signatures: A review. *IEEE Transactions on Instrumentation and Measurement*, 72, 1–19. https://doi.org/10.1109/TIM.2023.3285999
18. Liu Y., Wang Y., Li Y., Li Q., Wang J. (2022). SETR-YOLOv5n: A lightweight low-light lane curvature detection method based on fractional-order fusion model. *IEEE Access*, 10, 93003–93016. https://doi.org/10.1109/ACCESS.2022.3203443
19. Zhang J., Zhu D., Jian W., Hu W., Peng G., Chen Y., Wang Z. (2024). Fractional order complementary non-singular terminal sliding mode control of PMSM based on neural network. *International Journal of Automotive Technology*, 25(2), 213–224. https://doi.org/10.1007/s12239-024-00015-9
20. Sabir H., Ouassaid M., Ngote N. (2022). An experimental method for diagnostic of incipient broken rotor bar fault in induction machines. *Heliyon*, 8(3), 1–13. https://doi.org/10.1016/j.heliyon.2022.e09136
21. Pundir M., Kammer D. S. (2025). Simplifying FFT-based methods for solid mechanics with automatic differentiation. *Computer Methods in Applied Mechanics and Engineering*, 435, 117572. https://doi.org/10.1016/j.cma.2024.117572
22. Goolak S., Riabov I., Petrychenko O., Kyrychenko M., Pohosov O. (2025). The simulation model of an induction motor with consideration of instantaneous magnetic losses in steel. *Advances in Mechanical Engineering*, 17(2), 16878132251320236. https://doi.org/10.1177/16878132251320236
23. Trajin B., Chabert M., Regnier J., Faucher J. (2009). Hilbert versus Concordia transform for three-phase machine stator current time-frequency monitoring. *Mechanical systems and signal processing*, 23(8), 2648–2657. https://doi.org/10.1016/j.ymssp.2009.05.015

## REFERENCES:

1. Komorski P., Kominowski J., Motyl M. (2022). A proposal for a mobile system of vehicle and rail track diagnostics. *Transport Problems, 17*(2), 46–56. https://doi.org/10.20858/tp.2022.17.2.04
2. Gubarevych O., Goolak S., Golubieva S. (2022). Systematization and selection of diagnosing methods for the stator windings insulation of induction motors. *Revue Roumaine des sciences techniques—série électrotechnique et énergétique*, 67(4), 445–450.
3. Goolak S., Gorobchenko O., Holub H., Dudnyk Y. (2024). Increasing the efficiency of railway rolling stock operation with induction traction motors due to implementation of the operational system for diagnostic condition of rotor. *Diagnostyka*, 25(4), 1–11. https://doi.org/10.29354/diag/193809
4. Goolak S., Gubarevych O., Yurchenko V., Kyrychenko M. (2025). A review of diagnostic information processing methods in the construction of systems for operating diagnostics of rotor eccentricity of induction motors. *Diagnostyka*, 26(1), 1–15. https://doi.org/10.29354/diag/202757

5. Kumar A., Nanthaamornphong A., Gaur N., Masud M. (2025). Low complexity hybrid algorithm for improving PAPR BER and PSD in OTFS under diverse channel conditions. *Scientific Reports*, 15(1). 42023. https://doi.org/10.1038/s41598-025-26748-w

6. Mushtaq U., Khan A. A., Baig S., Ahmad M., Ribeiro M. V. (2025). SWIPT Enabled Wavelet Cooperative NOMA: Energy-Efficient Design Under Imperfect SIC. *Electronics*, 14(22). 4390. https://doi.org/10.3390/electronics14224390

7. Song Y., Yan J., Duan Z., Zhang L. (2025, July). Position Identification of Pmsm Based on Second-Order Generalized Integrator Under Hall Sensors Fault. In *2025 4th Conference on Fully Actuated System Theory and Applications (FASTA)* (pp. 1026–1031). IEEE. 10.1109/FASTA65681.2025.11138642

8. Liu H., Yang K., Liu L., Zheng Y., Cao X., Sun W., Zheng Y. (2025). Optimization of Energy Management Strategy for Hybrid Power System of Rubber-Tyred Gantry Cranes Based on Wavelet Packet Decomposition. *Energies*, 19(1), 139. https://doi.org/10.3390/en19010139

9. Tong F., Dong S., Lai J., Yuan X., Li X. (2022). Wall shear stress and wall heat flux in a supersonic turbulent boundary layer. *Physics of fluids*, 34(1). 015127. https://doi.org/10.1063/5.0079230

10. Andronis V., Karathanassi V., Tsalapati V., Kolokoussis P., Miltiadou M., Danezis C. (2022). Time series analysis of landsat data for investigating the relationship between land surface temperature and forest changes in Paphos Forest, Cyprus. *Remote Sensing*, 14(4), 1010. https://doi.org/10.3390/rs14041010

11. Wang Z. Z., Goh S. H. (2022). A maximum entropy method using fractional moments and deep learning for geotechnical reliability analysis. *Acta Geotechnica*, 17(4), 1147–1166. https://doi.org/10.1007/s11440-021-01326-2

12. Destrempes F., Cloutier G. (2023). Review of envelope statistics models for quantitative ultrasound imaging and tissue characterization. In *Quantitative ultrasound in soft tissues* (pp. 107–152). Cham: Springer International Publishing. https://doi.org/10.1007/978-3-031-21987-0_7

13. Plonka G., Potts D., Steidl G., Tasche M. (2023). Prony method for reconstruction of structured functions. In *Numerical Fourier Analysis* (pp. 567–620). Cham: Springer International Publishing. https://doi.org/10.1007/978-3-031-35005-4_10

14. Rozgić D., Petrović P. B. (2022). New modified DFT-Prony-based algorithms for removal of decaying DC components from fundamental phasor estimates. *Electrical Engineering*, 104(5), 3265–3279. https://doi.org/10.1007/s00202-022-01548-x

15. Aguilar J., Paulus L., Werbunat D., Grathwohl A., Waldschmidt C. (2025, March). Radon-Fourier Transform for Timing Correction in Uncoupled Digital Radar Networks. In *2025 16th German Microwave Conference (GeMiC)* (pp. 415–418). IEEE. https://doi.org/10.23919/GeMiC64734.2025.10979010

16. Xu T., Liu Y., Cui J., Jiang Y., He M., Miao D., Liu W., Li J. (2025). Calibration methods of optical path difference in optical frequency scanning interferometry with resampling resolving. *Measurement*, 248, 116854. https://doi.org/10.1016/j.measurement, 2025.116854

17. Niu G., Dong X., Chen Y. (2023). Motor fault diagnostics based on current signatures: A review. *IEEE Transactions on Instrumentation and Measurement*, 72, 1–19. https://doi.org/10.1109/TIM.2023.3285999

18. Liu Y., Wang Y., Li Y., Li Q., Wang J. (2022). SETR-YOLOv5n: A lightweight low-light lane curvature detection method based on fractional-order fusion model. *IEEE Access*, 10, 93003–93016. https://doi.org/10.1109/ACCESS.2022.3203443

19. Zhang J., Zhu D., Jian W., Hu W., Peng G., Chen Y., Wang Z. (2024). Fractional order complementary non-singular terminal sliding mode control of PMSM based on neural network. *International Journal of Automotive Technology*, 25(2), 213–224. https://doi.org/10.1007/s12239-024-00015-9

20. Sabir H., Ouassaid M., Ngote N. (2022). An experimental method for diagnostic of incipient broken rotor bar fault in induction machines. *Heliyon*, 8(3), 1–13. https://doi.org/10.1016/j.heliyon.2022.e09136

21. Pundir M., Kammer D. S. (2025). Simplifying FFT-based methods for solid mechanics with automatic differentiation. *Computer Methods in Applied Mechanics and Engineering*, 435, 117572. https://doi.org/10.1016/j.cma.2024.117572

22. Goolak S., Riabov I., Petrychenko O., Kyrychenko M., Pohosov O. (2025). The simulation model of an induction motor with consideration of instantaneous magnetic losses in steel. *Advances in Mechanical Engineering*, 17(2), 16878132251320236. https://doi.org/10.1177/16878132251320236

23. Trajin B., Chabert M., Regnier J., Faucher J. (2009). Hilbert versus Concordia transform for three-phase machine stator current time-frequency monitoring. *Mechanical systems and signal processing*, 23(8), 2648–2657. https://doi.org/10.1016/j.ymssp.2009.05.015

*Стаття надійшла до редакції: 18.10.2025; рецензування: 22.10.2025; прийнята до публікації 05.11.2025. Автори прочитали и дали згоду рукопису.*
*The article was submitted on 18.10.2025; revised on 22.10.2025; and accepted for publication on 05.11.2025. The authors read and approved the final version of the manuscript.*